HOKKAIDO UNIVERSITY

Title	Thermosensitive Seven-Coordinate Tb-III Complexes with LLCT Transitions
Author(s)	Ferreira da Rosa, Pedro Paulo; Nakanishi, Takayuki; Kitagawa, Yuichi et al.
Citation	European journal of inorganic chemistry, 2018(19), 2031-2037 https://doi.org/10.1002/ejic.201800281
Issue Date	2018-03-25
Doc URL	https://hdl.handle.net/2115/74367
Rights	This is the peer reviewed version of the following article: [Thermosensitive Seven‐Coordinate TbIII Complexes with LLCT Transitions], which has been published in final form at [10.1002/ejic.201800281]. This article may be used for non-commercial purposes in accordance with Wiley Terms and Conditions for Self-Archiving."
Type	journal article
File Information	Final manuscript - reviewe.pdf

Hokkaido University Collection of Scholarly and Academic Papers : HUSCAP

Thermo-sensitive luminophores using seven-coordinate Tb^{III} complexes based on LLCT transition

Pedro Paulo Ferreira da Rosa,[b] Takayuki Nakanishi,[a] Yuichi Kitagawa, [a] Tomohiro Seki, [a]

Hajime Ito, [a] Koji Fushimi, [a] and Yasuchika Hasegawa*[a]

Abstract: Seven-coordinate Tb^{III} complexes with strong-luminescence and thermo-sensing properties are reported. Mono-nuclear [Tb(tmh)$_3$(PEB)] (tmh: 2,2,6,6-tetramethyl-3,5-heptanedione, PEB: (diphenylphosphoryl)ethynyl)benzene)) and Di-nuclear [Tb$_2$(tmh)$_6$(*m*-BPEB)] (*m*-BPEB: 1,3-bis(diphenylphosphoryl)ethynyl)benzene) were characterized by single-crystal X-ray analysis. The quantum yields of [Tb(tmh)$_3$(PEB)] and [Tb$_2$(tmh)$_6$(*m*-BPEB)] were estimated to be 71 and 39 %, respectively. Thermo-sensing properties are evaluated by temperature depended emission lifetime measurements (Arrhenius analysis), which are affected by presence of ligand-to-ligand charge transfer (LLCT) bands. The LLCT bands are confirmed by DFT calculations.

Introduction

Luminescent metal complexes have attracted attention because of their versatile photophysical properties for applications such as displays[1–3], fluorescent lamps[4], LED lights[2,3,5–10], cellular probes and sensors.[11–17] The emission based on their charge transfer (CT) bands are strongly affected by the organic ligand moieties, coordination structure and coordination number. Various types of luminescent transition metal complexes have been reported, recently. Langton described that Ru^{II} complex with rotaxane units shows iodide recognition based on the enhancement of metal-ligand charge transfer (MLCT) emission.[18] The luminescence properties of Pt^{II} pyridyl complexes are depended strongly on the ligand-metal interaction and metal-metal-to-ligand charge transfer (MMLCT) transition.[19] Wärnmark demonstrated a Fe^{III} triazol complex showing room-temperature photoluminescence with enhanced emission lifetime through the doublet ligand-to-metal charge transfer (LMCT) transition.[20] Control of the ligand field is essential for the design of luminescent metal complexes.

The electronic transitions of luminescent lanthanide complexes are much different from those of transition metal complexes. Lanthanide complexes have characteristic photophysical properties derived from the metal centered 4*f*-4*f* transitions. The 4*f*-4*f* emission is based on the electric-dipole Laporte-forbidden transition with small offset, which leads to distinctive emission with high color purity (fwhm < 10 nm) and long emission lifetime (>1 μs).[21] It has been widely accepted that the 4*f*-4*f* intrinsically forbidden transitions can be partially allowed by mixing 5*d* states through the ligand field effect, based on the coordination structure. By the 4*f*-5*d* mixing, lanthanide complex with highly asymmetrical coordination structure exhibits large radiative rate constant (k_r).[22,23] We reported strong luminescent lanthanide complexes with asymmetric eight-coordinate square antiprism (8-SAP, D_{4d}), trigonal dodecahedron (8-TDH, D_{2d}), and nine-coordinate monocapped square antiprism (9-SAP, C_{4v}) structures.[24–26] Their coordination structures are composed of Eu^{III} ions, hexafluoroacetylacetonate and phosphine oxide ligands. The level of symmetry in the coordination structure of lanthanide complexes is important to improve their electronic transitions and luminescence.

In order to obtain new symmetric structures around the lanthanide ions, we successfully synthesized seven-coordinate Tb^{III} complex using sterically bulky tmh (2,2,6,6-tetramethyl-3,5-heptanedione) and TPPO (triphenylphosphine oxide) ligands that shows extremely high intrinsic emission quantum yield ([Tb(tmh)$_3$(TPPO)]: Φ_{ff} = 88%).[27] This high quantum yield is due to both the formation of asymmetric seven-coordinate structure (7-MCO, C_{3v}) and high triplet state energy level of tmh ligand. The asymmetric seven-coordination structure results in enlargement of the k_r of Tb^{III} complex. The large energy gap between emitting level of Tb^{III} ($^5D_4$) and excited triplet level of tmh (T_1) also leads to suppression of back energy transfer (BEnT), resulting in decrease of non-radiative rate constant (k_{nr}).[28] Seven-coordinate Tb^{III} complex with tmh and TPPO ligands provides high quantum yields with large k_r and small k_{nr} constants.

In this study, we present strong luminescent seven-coordinate Tb^{III} complexes with thermo-sensing properties. Various types of thermo-sensitive Tb^{III} complexes based on the thermal activation of BEnT have been reported.[29–31] Temperature-sensitive luminescent lanthanide complexes have potential applications in electronics, fluidics and aeronautical engineering[32] as responsive dyes.[33–37] Strong-luminescent seven-coordinate [Tb(tmh)$_3$(TPPO)], however, does not show the thermo-sensing property because of the suppression of BEnT process. Here, we designed novel seven-coordinate Tb^{III} complexes by introducing ethynyl groups in the phosphine oxide ligand in order to promote new energy transfer pathways (Figure 1a). The ethynyl group in the phosphine oxide ligands expands the π-conjugation system, which stabilizes their excited states. This stabilization allows interaction between tmh and phosphine oxide ligand for formation of ligand-to-ligand charge transfer

[a] Dr. Y. Kitagawa, Dr. T. Nakanishi, Dr. T. Seki, Prof. K. Fushimi, Prof. H. Ito, Prof. Y. Hasegawa
Faculty of Engineering
Hokkaido University
Kita-13 Jo, Nishi-8 Chome, Sapporo, Hokkaido 060-8628 (Japan)
E-mail: hasegaway@eng.hokudai.ac.jp

[b] Mr. P.P. Ferreira da Rosa
Graduate School of Chemical Sciences and Engineering
Hokkaido University
Kita-13 Jo, Nishi-8 Chome, Sapporo, Hokkaido 060-8628 (Japan)

Supporting information for this article is given via a link at the end of the document

(LLCT) band. New energy transfer pathway using LLCT band induces thermo-sensing properties in seven-coordinate Tb^{III} complexes (Figure 1b).

Mono- and di-nuclear seven-coordinate Tb^{III} complexes with ethynyl introduced phosphine oxides, PEB ((diphenylphosphoryl)ethynyl)benzene) and *m*-BPEB (1,3-bis(diphenylphosphoryl)ethynyl)benzene), were synthesized (Figure 1c and 1d). Previously reported seven-coordinate $[Tb(tmh)_3(TPPO)]$ was also prepared as a reference.[27] Their coordination structures were characterized using single-crystal X-ray diffraction analysis. Luminescence performances of the Tb^{III} complexes were evaluated using emission spectra, total emission quantum yields and emission lifetimes. Their temperature-sensitivities are estimated using temperature depended emission lifetime measurements (Arrhenius analysis). We also discuss about LLCT characteristics from density functional theory (DFT) calculations. The seven-coordinate Tb^{III} complex with ethynyl group exhibits remarkable LLCT-assisted thermo-sensitive luminescence, while maintaining high emission quantum yield. The conceptual molecular design for strong luminescent and thermo-sensitive Tb^{III} complex can expand the frontier field of coordination chemistry, photophysics and material science.

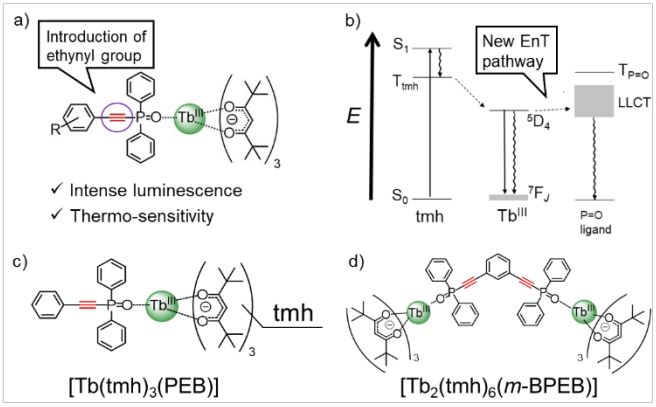

Figure 1. (a) Conceptual molecular design, (b) Energy diagram of Tb^{III} complexes with ethynyl group, (c) Mono-nuclear $[Tb(tmh)_3(PEB)]$, and (d) Di-nuclear $[Tb_2(tmh)_6(m\text{-BPEB})]$.

Results and Discussion

Structure

Seven-coordinate $[Tb(tmh)_3(PEB)]$ (Tb-PEB) and $[Tb_2(tmh)_6(m\text{-BPEB})]$ (Tb-BPEB) were synthesized by the complexation of phosphine oxide ligands (PEB and *m*-BPEB) with precursor $[Tb_2(tmh)_6]$[38] in methanol for 12 h (see Supporting Information, Scheme S1). $[Tb(tmh)_3(TPPO)]$ (Tb-TPPO) was also synthesized by the same method for comparison with Tb^{III} complexes using ethynyl groups. The single crystals of Tb-PEB and Tb-BPEB were obtained by recrystallization from methanol solution. The structures of Tb-PEB and Tb-BPEB were determined by single-crystal X-ray analyses (Figure 2a and 2b). The Tb-PEB is composed of one phosphine oxide ligand (PEB) and $Tb(tmh)_3$ unit forming a seven-coordinate structure. For di-nuclear Tb-BPEB, two $Tb(tmh)_3$ units are bridged by *m*-BPEB ligand. The selected bond length between Tb^{III} and O (phosphine oxide) in Tb-PEB and Tb-BPEB were 2.31 and 2.35 Å, respectively. Their bond lengths are similar to that in Tb-TPPO (2.31 Å). We also found specific intermolecular CH/O and π/π interactions that are only observed in the Tb-PEB structure (Figure 2c). The selected distances and angles between the Tb^{III} and the O atoms directly reflect the coordination geometry of the complex. Based on the crystal structures, we performed continuous shape measures (CShM) calculations using SHAPE[39–41] to determine the coordination geometrical structures around the Tb^{III} ions in the first coordination sphere. The S_{CShM} criterion represents the degree of deviation from ideal coordination structure and is given by Equation (1):

$$S_{CShM} = \min \frac{\sum_k^N |Q_k - P_k|^2}{\sum_k^N |Q_k - Q_0|^2} \times 100 \qquad (1)$$

where Q_k is the vertices of an actual structure, Q_0 is the center of mass of an actual structure, P_k is the vertices of an ideal structure, and N is the number of vertices. The estimated S_{CShM} values of the Tb^{III} complexes are summarized in Table S2. On the basis of the minimal value of S_{CShM}, the pseudo-coordination polyhedral structures of Tb-PEB and Tb-BPEB were categorized to be 7-MCTP (monocapped-trigonal prismatic, point group: C_{2v}) and 7-MCO (monocapped-octahedral, point group: C_{3v}), respectively. Tb-TPPO was characterized as 7-MCO in a previous report.[27] The asymmetric Tb-PEB with C_{2v} point group is expected to provide high emission quantum yield related to larger k_r.

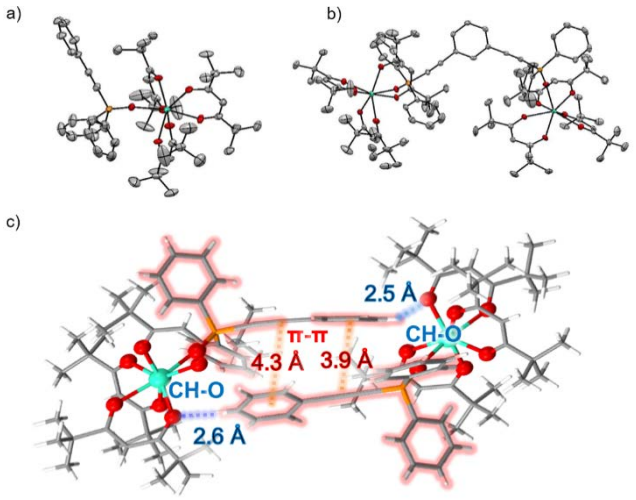

Figure 2. Perspective view of (a) Tb-PEB and (b) Tb-BPEB without hydrogen atoms, showing 50% probability displacement ellipsoids. (c) Representation of intermolecular CH/O and π/π interactions in Tb-PEB.

Photophysical properties

Excitation and emission spectra of Tb-PEB and Tb-BPEB in solids are shown in Figure 3a. The transition bands at around 350 nm in excitation spectra are assigned to π-π* and/or σ-π* transitions of the organic tmh ligands. The shoulder bands at approximately 380 nm are due to 4*f*-4*f* transitions of Tb^{III} ($^5G_6$, $^5D_3 \leftarrow {}^7F_6$).[42] The emission bands at 490, 544, 582, 615 and 642 nm are caused by typical 4*f*-4*f* transitions of Tb^{III} ions ($^5D_4 \rightarrow {}^7F_J$ (*J* = 6,5,4,3 and 2)), respectively. The spectral shapes including the stark splittings of Tb-PEB and Tb-BPEB are much similar to those of Tb-TPPO and previous Tb^{III} complexes with low-symmetrical seven-coordinate structures (see Supporting Information, Figure S1).[27,43,44]

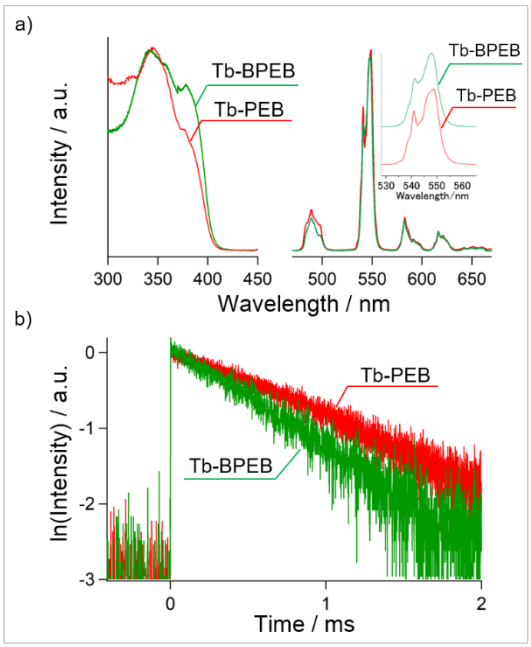

Figure 3. (a) Excitation and emission spectra of Tb-PEB (red line) and Tb-BPEB (green line) in solids at room temperature. Excitation spectra were recorded in respect to emission at 544 nm ($^5D_4 \rightarrow {}^7F_6$) and were normalized at 350 nm. Emission spectra were excited at 350 nm. (b) Emission decay profiles of Tb-PEB (red line) and Tb-BPEB (green line) in solids at room temperature excited at 355 nm (Nd:YAG 3ω).

Time-resolved emission profiles of Tb-PEB and Tb-BPEB at room temperature reveal single-exponential decays with millisecond scale lifetimes. The emission lifetimes observed from the $^5D_4$ excited level (τ_{obs}) were determined from the slope of the logarithmic decay profiles (Figure 3b). Total emission quantum yields Φ_{tot} for excitation at 360 nm were directly measured with an integrating-sphere unit. The τ_{obs} and Φ_{tot} of Tb-PEB, Tb-BPEB and Tb-TPPO are summarized in Table 1. The Φ_{tot} is composed of intrinsic emission quantum yield (Φ_{ff}) and energy transfer efficiency (η_{sens}) as expressed in Equation 2. The τ_{obs} is also directly related to Φ_{ff} by Equation 3.

$$\Phi_{tot} = \Phi_{ff} \times \eta_{sens} \quad (2)$$

$$\tau_{obs} = \frac{\Phi_{ff}}{k_r} = \frac{1}{k_r + k_{nr}}, \quad \Phi_{ff} = \frac{k_r}{k_r + k_{nr}} \quad (3)$$

In our experiments, the τ_{obs} and Φ_{tot} of Tb-PEB were larger than those of Tb-TPPO. According to X-ray analysis and continuous shape factor calculations, the coordination geometry of Tb-PEB was categorized to be monocapped-trigonal prismatic structure (7-MCTP, point groups: C_{2v}). The combination of asymmetric C_{2v} structure and tight-packed molecular interactions (CH/O and π/π) should provide a larger k_r and smaller k_{nr}, respectively. The larger k_r and smaller k_{nr} enhances the Φ_{ff} of Tb-PEB, which provides longer τ_{obs} according to Equation 3.

The τ_{obs} and Φ_{tot} of Tb-BPEB are estimated as 0.81 ms and 39 %, respectively. The Φ_{tot} in Tb-BPEB is smaller than those of Tb-TPPO, although their τ_{obs} and coordination structure (7-MCO, point groups: C_{3v}) are similar to those of Tb-TPPO. We propose that the smaller Φ_{tot} of Tb-BPEB is due to inefficient energy transfer (small η_{sens}) related to the presence of new energy transfer pathways in the ethynyl-introduced Tb^{III} complex.

Table 1. Photophysical properties

Name	Chemical formula	Point group (geometry)	τ_{obs}[a] /ms	Φ_{tot}[b] / %	A[c] / s^{-1}	E_a[c] / cm^{-1}
Tb-PEB	$[Tb(tmh)_3$ (PEB)]	C_{2v} (7-MCTP)	1.2	71	1.1×10^8	3.6×10^3
Tb-BPEB	$[Tb_2(tmh)_6$ (*m*-BPEB)]	C_{3v} (7-MCO)	0.81	39	9.3×10^8	3.8×10^3
Tb-TPPO	$[Tb(tmh)_3$ (TPPO)][27]	C_{3v} (7-MCO)	0.73	66	–	–

[a] Emission lifetime (τ_{obs}) of the Tb^{III} complexes were measured by excitation at 355 nm (Nd:YAG 3ω) at room temperature. [b] Total emission quantum yield (excited at 360 nm). [c] $\ln(1/\tau_{obs} - 1/\tau_{100K}) = \ln(k_{EnT}) = \ln(A) - (E_a/k_B T)$.

DFT calculations

The new energy transfer pathway in Tb^{III} complexes with ethynyl group was investigated using TD-DFT calculations (B3LYP, 6-31G(d)) of excited Tb-TPPO and Tb-PEB using Al^{III} ions instead of Tb^{III} ions. Their molecular orbital representations by Natural Transition Orbitals (NTO) are shown in Figure 4a and 4b (Complementary data: see Figure S2-S5). The NTO images and energy levels of Tb-BPEB were also calculated (see Supporting Information, Figure S6-S7). The electron densities for S_0-S_1 and S_0-T_1 transitions of Tb-TPPO are localized in π orbitals of tmh ligands (Figure 4a). On the other hand, the electron densities in ground and excited states of Tb-PEB are located at tmh and PEB ligand, respectively. These transitions from Tb-PEB are interpreted to be ligand-to-ligand charge transfer (LLCT) transitions. The energy levels of the lowest excited singlet (S_1) and triplet (T_1) states of Tb-TPPO, Tb-PEB and Tb-BPEB were

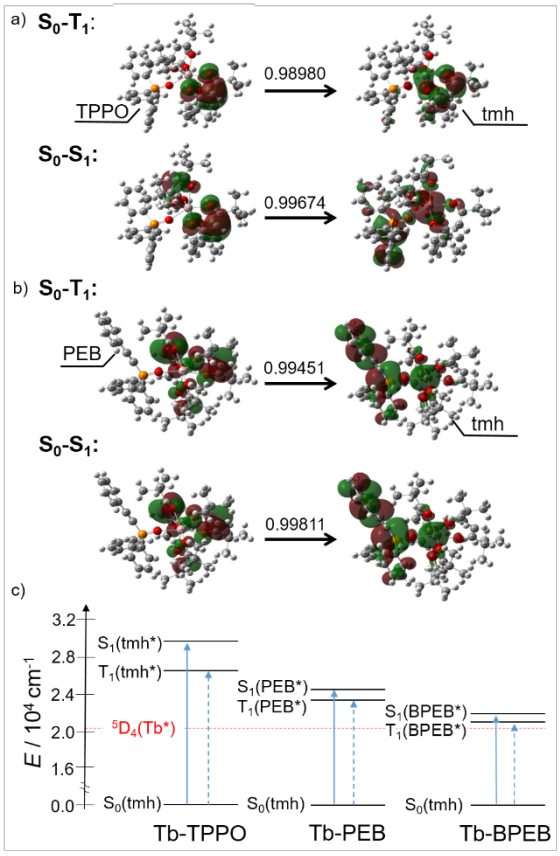

Figure 4. Molecular orbital representations of the lowest triplet and singlet excited states of (a) Tb-TPPO and (b) Tb-PEB simplified by NTO showing the highest transition probability. (c) Energy diagram for the lowest triplet and singlet excited states for Tb-TPPO, Tb-PEB and Tb-BPEB. DFT calculations were performed using Al^{III} ions instead of Tb^{III} ions for all complexes.

summarized in Figure 4c.

With the introduction of the ethynyl group in phosphine oxides, their π-conjugation systems were expanded allowing for the effective stabilization of LUMO (HOMO and LUMO levels: see Supporting Information, Table S3 and Figure S8). The lower LUMO in PEB and *m*-BPEB facilitates the interaction between tmh and phosphine oxide ligand for formation of ligand-to-ligand charge transfer (LLCT) bands (frequency oscillator of S_0-S_1 and S_0-T_1 transition: see Table S4-S6); the oscillator strengths of LLCT bands are explained using calculated and measured absorption spectra: see Figure S9). These charge transfer bands in Tb-PEB and Tb-BPEB provide new energy transfer pathways in lower energetic levels, which are closer to the Tb^{III} excited states ($^5D_4$: 20500 cm^{-1}).[42]

Thermo-sensitivity

Thermo-sensitive measurements through change in emission lifetime have been reported as a precise and reliable evaluation for estimation of performance in thermo-sensors.[45–48]

Temperature-depended emission lifetimes were measured to investigate the temperature sensitivity of the Tb^{III} complexes (Figure 5a). The emission lifetimes of Tb-TPPO were also measured as a reference. Tb-TPPO did not show any change in the emission lifetime from 100 to 400 K. We found that Tb^{III} complexes with ethynyl groups showed decrease in the emission lifetime from 340 to 400 K. These emission lifetimes changes are caused by the energy transfer to the LLCT transitions in Tb-PEB and Tb-BPEB. This quenching process is depended on the energy-transfer rate k_{EnT}.

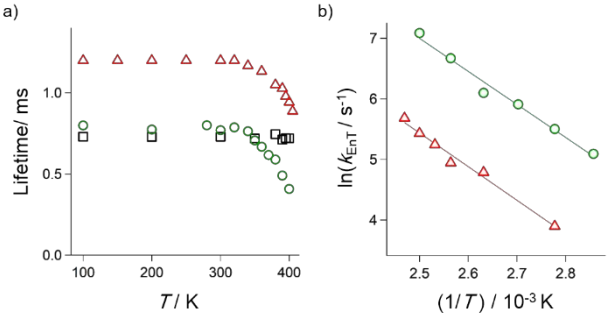

Figure 5. (a) Temperature-depended emission lifetimes of Tb-TPPO (black square), Tb-PEB (red triangle) and Tb-BPEB (green circle) excited at 355 nm (Nd:YAG 3ω), and the (b) Arrhenius plot for energy-transfer rate of Tb-PEB (red triangle) and Tb-BPEB (green circle). Arrhenius equation: $\ln(1/\tau_{obs} - 1/\tau_{100K}) = \ln(k_{EnT}) = \ln(A) - (E_a/k_B T)$.

From the Arrhenius plots of the energy-transfer rate k_{EnT} from the $^5D_4$ to the LLCT state, the activation energy E_a and the frequency factor A were estimated (Figure 5b, Table 1). The E_a of Tb-PEB (3.6×10^3 cm^{-1}) are similar to that of Tb-BPEB (3.8×10^3 cm^{-1}). We consider that thermo-quenching process from $^5D_4$ excited state of Tb^{III} to the LLCT state in Tb-PEB is similar to that of Tb-BPEB.

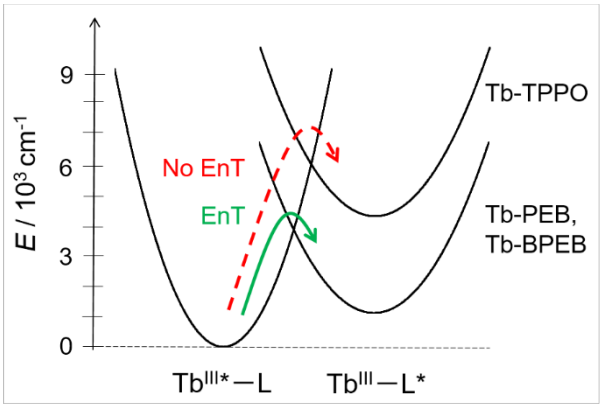

Figure 6. Potential curves showing the energy transfer from Tb^{III} excited state ($^5D_4$) to the ligands' excited states.

In order to understand the thermo-sensitivity of Tb-PEB and Tb-BPEB, the potential curves of those complexes were

hypothesized (Figure 6). The left potential curve in Figure 6 is a combination of excited $^5D_4$ (Tb^{III}) and grounded S_0 (tmh) states, Tb^{III}*-L. The right potential curves are composed of grounded $^7F_6$ (Tb^{III}) and excited states of ligands, Tb^{III}-L*. Here, we normalized the energy level of left curve for comparison of activation energy in energy transfer process (thermo-sensitivity). The cross-points represent the activation energies (E_a). In the case of Tb-PEB and Tb-BPEB, the energy level of right potential curve is decreased by the formation of LLCT transitions, resulting in smaller E_a. The smaller E_a leads to effective thermo-sensing property in seven-coordinate Tb^{III} complex. On the other hand, Tb-TPPO does not show thermo-sensitivity because of the high energy level in which the cross-point is situated.

The A values for Tb-PEB and Tb-BPEB are 1.1×10^8 and 9.3×10^8 s^{-1}, respectively. The A value is affected by the electronic coupling of the $^5D_4$ configuration with the LLCT state. This calculation results indicate that the degree of electronic coupling of $^5D_4$ and the LLCT state for Tb-PEB is smaller than that of Tb-BPEB. The E_a and A values of seven-coordinate Tb^{III} complex are depended on the presence of LLCT band. We successfully observed thermo-sensing ability in Tb^{III} complexes with ethynyl groups.

Conclusion

Novel mono- and di-nuclear seven-coordinate Tb^{III} complexes with ethynyl groups in the phosphine oxide ligand were synthesized. Tb-PEB showed remarkable total emission quantum yield due to a large k_r and small k_{nr} from an asymmetrical coordination structure and strong intermolecular interactions. We also successfully demonstrated the thermo-sensing properties of Tb-PEB and Tb-BPEB from 340 to 400 K. These thermo-sensing properties are enabled by the introduction of ethynyl groups in the phosphine oxide ligand. DFT calculations of Tb-PEB and Tb-BPEB prove the formation of ligand-to-ligand charge transfer (LLCT) band from tmh to phosphine oxide ligands. We consider that new energy transfer pathway using LLCT band induces thermo-sensing properties in seven-coordinate Tb^{III} complexes. Highly luminescent seven-coordinate Tb^{III} complexes with thermo-sensitive properties have the potential to break new ground in fields of coordination chemistry, thermodynamics and photophysical science.

Experimental Section

General Methods: All chemicals were reagent grade and used without further purification. Infrared spectra were recorded on a JASCO FT/IR-420 spectrometer. ESI-MS spectra were measured using a JEOL JMS-T100LP and a Thermo Scientific Exactive. Elemental analyses were performed on a J-Science Lab JM 10 Micro Corder and an Exeter Analytical CE440. ^{1}H NMR (400 MHz) spectra were recorded on a JEOL ECS400. ^{13}C NMR (100 MHz) and ^{31}P NMR (162 MHz) spectra were recorded on a JEOL ECX400. Chemical shifts were reported in δ ppm, referenced to an internal tetramethylsilane standard for ^{1}H NMR and internal 85% H_3PO_4 standard for ^{31}P NMR.

Preparation of (diphenylphosphoryl)ethynyl)benzene (PEB): Ethynylbenzene (**A**, 1.02 g, 10 mmol) was dissolved in dry THF (60 mL), and a solution of *n*-BuLi (7.5 mL, 1.6 M hexane, 12 mmol) was added dropwise at -80 °C in ca. 15 min. The mixture was allowed to stir for 3h at -10 °C, after which (2.28 mL, 12 mmol) was added dropwise at -80 °C. The mixture was gradually brought to room temperature and stirred for 15 h. The product was extracted with dichloromethane, washed with brine three times, and dried over with anhydrous $MgSO_4$. The solvent was evaporated, and the obtained pale white solid was placed with dichloromethane (30 mL) in a flask. The solution was cooled to 0 °C, and then 30% H_2O_2 aqueous solution (5 mL) was added to it. The reaction mixture was stirred for 3 h. The product was extracted with dichloromethane; the extracts were purified by column chromatography on SiO_2 using ethyl acetate and hexane as mixed eluent (silica gel, ethyl acetate:hexane = 3:1) to afford PEB.

Yield: 1.45 g (48%). ^{1}H NMR (400 MHz, $CDCl_3$, 25°C): δ 7.87-7.94 (q, 4H, -CH), δ 7.62-7.43 (m, 9H, -CH), δ 7.36-7.41 (t, 2H, -CH) ppm. ^{13}C NMR (100 MHz, $CDCl_3$, 25°C): δ 133.8, 132.7, 132.4, 131.2, 131.1, 130.8, 128.9, 128.7, 83.8, 82.1 ppm. ^{31}P NMR (162 MHz, $CDCl_3$, 25°C): δ 8.96 (s, 1P) ppm. ESI-MS (*m/z*): calcd. for $C_{20}H_{16}OP$ $[PEB+H]^+$: 303.09, found 303.09. Elemental analysis calcd.(%) for $C_{20}H_{15}OP$: C, 79.46; H, 5.00. Found C, 79.13; H, 4.92.

Preparation of 1,3-bis(diphenylphosphoryl)ethynyl)benzene (*m*-BPEB): 1,3-diethynylbenzene (**B**, 1.26 g, 10 mmol) was dissolved in dry THF (60 mL), and a solution of *n*-BuLi (15 mL, 1.6 M hexane, 24 mmol) was added dropwise at -80 °C in ca. 15 min. The mixture was allowed to stir for 3h at -10 °C, after which (4.56 mL, 24 mmol) was added dropwise at -80 °C. The mixture was gradually brought to room temperature and stirred for 15 h. The product was extracted with dichloromethane, washed with brine three times, and dried over with anhydrous $MgSO_4$. The solvent was evaporated, and the obtained pale white solid was placed with dichloromethane (30 mL) in a flask. The solution was cooled to 0 °C, and then 30% H_2O_2 aqueous solution (10 mL) was added to it. The reaction mixture was stirred for 3 h. The product was extracted with dichloromethane; the extracts were washed with ethyl acetate to afford a white powder. The powder was recrystallized from methanol to give colorless chunk-shaped crystals.

Yield: 2.61g (49.6%). ^{1}H NMR (400 MHz, $CDCl_3$, 25°C): δ 7.85-7.92 (q, 8H, -CH), δ 7.82 (s, 1H, -CH), δ 7.65-7.68 (d, 2H, -CH), δ 7.48-7.60 (m, 12H, -CH), δ 7.40-7.44 (t, 1H, -CH) ppm. ^{13}C NMR (100 MHz, $CDCl_3$, 25°C): δ 136.3, 134.4, 133.3, 132.6, 132.1, 131.2, 131.1, 129.2, 129.0, 128.8, 85.4, 83.7 ppm. ^{31}P NMR (162 MHz, $CDCl_3$, 25°C): δ 9.15 (s, 2P) ppm. ESI-MS (m/z): calcd. for $C_{34}H_{25}P_2O_2$ [*m*-BPEB+H]$^+$: 527.13, found 527.13. Elemental analysis calcd.(%) for $C_{34}H_{24}P_2O_2$: C, 77.56; H, 4.59. Found C, 77.51; H, 4.48.

Preparation of $[Tb(tmh)_3(TPPO)]$ (Tb-TPPO), $[Tb(tmh)_3(PEB)]$ (Tb-PEB), $[Tb_2(tmh)_6$(*m*-BPEB)] (Tb-BPEB): The precursor complex, $[Tb_2(tmh)_6]$, was synthesized as described in previous report.[38] $[Tb_2(tmh)_6]$ (0.87 g, 0.6 mmol), and phosphine oxide ligands (TPPO: 0.33 g, 1.2 mmol; PEB: 0.36 g, 1.2 mmol; *m*-BPEB: 0.32 g, 0.6 mmol) were dissolved in methanol. The solutions were heated at reflux while stirring for 12 h. The solution was concentrated by an evaporator, and then filtrated with addition of new methanol into solution. That mixture was left to recrystallize giving colorless crystals.

$[Tb(tmh)_3(TPPO)]$ (Tb-TPPO): Yield: 0.48 g (40%). IR (ATR) $\tilde{\nu}$ = 2835-3002 (m, C-H), 1573 (s, C=O), 1194 (s, P=O). ESI-MS (m/z): calcd. for $C_{51}H_{73}O_7PTb$ $[(Tb\text{-}TPPO)+H]^+$: 987.42, found 987.43. Elemental analysis calcd.(%) for $C_{51}H_{72}O_7PTb$: C, 62.06; H, 7.35. Found C, 62.02; H, 7.30.

[Tb(tmh)$_3$(PEB)] (Tb-PEB): Yield: 0.28 g (23%). IR (ATR) $\tilde{\upsilon}$ = 2835-3002 (m, C-H), 1571 (s, C=O), 1194 (s, P=O). ESI-MS (m/z): calcd. for $C_{42}H_{53}O_5PTb[(Tb\text{-}PEB)\text{-}tmh]^+$: 827.29, found 827.30. Elemental analysis calcd.(%) for $C_{53}H_{72}O_7PTb$: C, 62.96; H, 7.18. Found C, 62.77; H, 7.16.

[Tb$_2$(tmh)$_6$(*m*-BPEB)] (Tb-BPEB): Yield: 0.24 g (20%). IR (ATR) $\tilde{\upsilon}$ = 2832-3002 (m, C-H), 1571 (s, C=O), 1190 (s, P=O). ESI-MS (m/z): calcd. for $C_{78}H_{101}O_{10}P_2Tb_2$ [(Tb-BPEB)-2tmh+H]$^+$: 1577.45, found 1577.44. Elemental analysis calcd.(%) for $C_{100}H_{138}O_{14}P_2Tb_2$: C, 61.79; H, 7.16. Found C, 61.63; H, 7.19.

Optical Measurements: Emission and excitation spectra were recorded on a HORIBA Fluorolog-3 spectrofluorometer and corrected for the response of the detector system. Emission lifetimes (τ_{obs}) were measured using the third harmonics (355 nm) of a Q-switched Nd:YAG laser (Spectra Physics, INDI-50, fwhm = 5 ns, λ = 1064 nm) and a photomultiplier (Hamamatsu photonics, R5108, response time ≤ 1.1 ns). The Nd:YAG laser response was monitored with a digital oscilloscope (Sony Tektronix, TDS3052, 500 MHz) synchronized to the single-pulse excitation. Emission lifetimes were determined from the slope of logarithmic plots of the decay profiles. The emission quantum yields excited at 360 nm (Φ_{tot}) were estimated using a JASCO F-6300-H spectrometer attached with JASCO ILF-533 integrating sphere unit (φ = 100 nm). The wavelength dependence of the detector response and the beam intensity of the Xe light source for each spectrum were calibrated using a standard light source.

Crystallography: The X-ray crystal structures and crystallographic data for Tb-PEB and Tb-BPEB are shown in Figure 2a, 2b and Table S1. Tb-TPPO is also shown in Table S1 for reference. All measurements were made on a Rigaku RAXIS RAPID or Rigaku XtaLAB PRO MM007 imaging plate area detector with graphite monochromatic Mo-K_α radiation. Correction for decay and Lorentz-polarization effects were made using empirical absorption correction, solved by direct methods and expanded using Fourier techniques. Non-hydrogen atoms were refined anisotropically using SHELX system. Hydrogen atoms were refined using the riding model. All calculations were performed using the crystal structure crystallographic and Olex 2 software package. The CIF data was confirmed by the checkCIF/PLATON service. CCDC-1823898 (for Tb-PEB) and CCDC-1823897 (for Tb-BPEB) contain the supplementary crystallographic data for this paper. These data can be obtained free of charge from The Cambridge Crystallographic Data Centre via www.ccdc.cam.ac.uk/data_request/cif.

Computational methods: To investigate the LLCT transitions in the Tb^{III} complex, DFT calculation was performed. Al^{III} ions were used instead of Tb^{III} ions. The energy calculations from the structures obtained from crystallography were carried out using the Gaussian 09 program package[49] at the B3LYP level with the basis set 6-31G(d). From time-depended calculations, each excited state was characterized by simplified Natural Transition Orbitals[50] and compared in respect to their energy levels.

Acknowledgements

We appreciate the support of Rigaku Corporation for single crystal X-ray analyses and crystallography measurements.

Keywords: Terbium • Luminescence • Lanthanide • Thermo-sensing • Charge-transfer

[1] J. Gil-Rostra, F. J. Ferrer, J. P. Espinós, A. R. González-Elipe, F. Yubero, *ACS Appl. Mater. Interfaces* **2017**, *9*, 16313–16320.
[2] V. V. Rangari, S. J. Dhoble, *J. Rare Earths* **2015**, *33*, 140–147.
[3] P. Du, L. Krishna Bharat, J. S. Yu, *J. Alloys Compd.* **2015**, *633*, 37–41.
[4] D. Hou, W. Chen, X. Ding, H. Liang, L. Zheng, J. Zhang, *ECS J. Solid State Sci. Technol.* **2013**, *2*, R79–R81.
[5] H. Xu, J. Wang, Y. Wei, G. Xie, Q. Xue, Z. Deng, W. Huang, *J. Mater. Chem. C* **2015**, *3*, 1893–1903.
[6] H. Xu, K. Yin, W. Huang, *Chem. Eur. J.* **2007**, *13*, 10281–10293.
[7] Q. Ling, Y. Song, S. J. Ding, C. Zhu, D. S. H. Chan, D. L. Kwong, E. T. Kang, K. G. Neoh, *Adv. Mater.* **2005**, *17*, 455–459.
[8] Z. Ahmed, K. Iftikhar, *RSC Adv.* **2014**, *4*, 63696–63711.
[9] H. Wang, P. He, H. Yan, J. Shi, M. Gong, *Inorg. Chem. Commun.* **2011**, *14*, 1183–1185.
[10] D. Yang, Y. Xu, Y. Yao, J. Zhang, J. Wang, Y. Wang, *Synth. Met.* **2016**, *221*, 236–241.
[11] C. Reichardt, K. R. A. Schneider, T. Sainuddin, M. Wächtler, S. A. McFarland, B. Dietzek, *J. Phys. Chem. A* **2017**, *121*, 5635–5644.
[12] K. Szaciłowski, W. Macyk, A. Drzewiecka-Matuszek, M. Brindell, G. Stochel, *Chem. Rev.* **2005**, *105*, 2647–2694.
[13] D. Cioloboc, C. Kennedy, E. N. Boice, E. R. Clark, D. M. Kurtz, *Biomacromolecules* **2018**, *19*, 178–187.
[14] M. Martínez, M. P. Carranza, A. Massaguer, L. Santos, J. A. Organero, C. Aliende, R. De Llorens, I. Ng-Choi, L. Feliu, M. Planas, et al., *Inorg. Chem.* **2017**, *56*, 13679–13696.
[15] G. Muller, *Dalt. Trans.* **2009**, *0*, 9692–9707.
[16] J. Jia, Y. Zhang, M. Zheng, C. Shan, H. Yan, W. Wu, X. Gao, B. Cheng, W. Liu, Y. Tang, *Inorg. Chem.* **2018**, *57*, 300–310.
[17] M. C. Heffern, L. M. Matosziuk, T. J. Meade, *Chem. Rev.* **2014**, *114*, 4496–4539.
[18] M. J. Langton, I. Marques, S. W. Robinson, V. Félix, P. D. Beer, *Chem. Eur. J.* **2016**, *22*, 185–192.
[19] K. Li, G. S. Ming Tong, Q. Wan, G. Cheng, W.-Y. Tong, W.-H. Ang, W.-L. Kwong, C.-M. Che, *Chem. Sci.* **2016**, *7*, 1653–1673.
[20] P. Chábera, Y. Liu, O. Prakash, E. Thyrhaug, A. El Nahhas, A. Honarfar, S. Essén, L. A. Fredin, T. C. B. Harlang, K. S. Kjær, et al., *Nature* **2017**, *543*, 695–699.
[21] A. de Bettencourt-Dias, *Dalt. Trans.* **2007**, *0*, 2229–2241.
[22] M. H. V. Werts, R. T. F. Jukes, J. W. Verhoeven, *Phys. Chem. Chem. Phys.* **2002**, *4*, 1542–1548.
[23] K. Binnemans, R. Van Deun, C. Gorller-Walrand, S. R. Collinson, F. Martin, D. W. Bruce, C. Wickleder, *Phys. Chem. Chem. Phys.* **2000**, *2*, 3753–3757.
[24] K. Miyata, T. Nakagawa, R. Kawakami, Y. Kita, K. Sugimoto, T. Nakashima, T. Harada, T. Kawai, Y. Hasegawa, *Chem. Eur. J.* **2011**, *17*, 521–528.
[25] K. Miyata, Y. Hasegawa, Y. Kuramochi, T. Nakagawa, T. Yokoo, T. Kawai, *Eur. J. Inorg. Chem.* **2009**, *2009*, 4777–4785.
[26] K. Miyata, T. Nakanishi, K. Fushimi, Y. Hasegawa, *J. Photochem. Photobiol. A Chem.* **2012**, *235*, 35–39.
[27] K. Yanagisawa, T. Nakanishi, Y. Kitagawa, T. Seki, T. Akama, M. Kobayashi, T. Taketsugu, H. Ito, K. Fushimi, Y. Hasegawa, *Eur. J. Inorg. Chem.* **2015**, *2015*, 4769–4774.

[28] M. Latva, H. Takalo, V.-M. Mukkala, C. Matachescu, J. C. Rodríguez-Ubis, J. Kankare, *J. Lumin.* **1997**, *75*, 149–169.

[29] C. Piguet, A. F. Williams, G. Bernardinelli, E. Moret, J. G. Bünzli, *Helv. Chim. Acta* **1992**, *75*, 1697–1717.

[30] N. Armaroli, G. Accorsi, F. Barigelletti, S. M. Couchman, J. S. Fleming, N. C. Harden, J. C. Jeffery, K. L. V. Mann, J. A. McCleverty, L. H. Rees, et al., *Inorg. Chem.* **1999**, *38*, 5769–5776.

[31] T. Kajiwara, K. Katagiri, M. Hasegawa, A. Ishii, M. Ferbinteanu, S. Takaishi, T. Ito, M. Yamashita, N. Iki, *Inorg. Chem.* **2006**, *45*, 4880–4882.

[32] J. B. Barlow, W. H. Rae, A. Pope, A. Pope, *Low-Speed Wind Tunnel Testing*, Wiley, **1999**.

[33] Y. Cui, H. Xu, Y. Yue, Z. Guo, J. Yu, Z. Chen, J. Gao, Y. Yang, G. Qian, B. Chen, *J. Am. Chem. Soc.* **2012**, *134*, 3979–3982.

[34] P. C. R. Soares-Santos, L. Cunha-Silva, F. A. Almeida Paz, R. A. Sa Ferreira, J. Rocha, T. Trindade, L. D. Carlos, H. I. S. Nogueira, *Cryst. Growth Des.* **2008**, *8*, 2505–2516.

[35] K. Miyata, Y. Konno, T. Nakanishi, A. Kobayashi, M. Kato, K. Fushimi, Y. Hasegawa, *Angew. Chemie - Int. Ed.* **2013**, *52*, 6413–6416.

[36] S. Katagiri, Y. Hasegawa, Y. Wada, S. Yanagida, *Chem. Lett.* **2004**, *33*, 1438–1439.

[37] K. Binnemans, *Chem. Rev.* **2009**, *109*, 4283–4374.

[38] F. Fulgêncio, F. C. De Oliveira, F. F. Ivashita, A. Paesano, D. Windmöller, A. Marques-Netto, W. F. Magalhães, J. C. MacHado, *Spectrochim. Acta - Part A Mol. Biomol. Spectrosc.* **2012**, *92*, 415–418.

[39] D. Casanova, M. Llunell, P. Alemany, S. Alvarez, *Chem. Eur. J.* **2005**, *11*, 1479–1494.

[40] M. Pinsky, D. Avnir, *Inorg. Chem.* **1998**, *37*, 5575–5582.

[41] Universitat de Barcelona, “Electronic Structure Group - SHAPE 2.1,” can be found under http://www.ee.ub.edu/index.php?option=com_content&view=article&id=575:shape-available&catid=80:news&Itemid=466, **2013**.

[42] W. T. Carnall, P. R. Fields, K. Rajnak, *J. Chem. Phys.* **1968**, *49*, 4447–4449.

[43] K. Yanagisawa, Y. Kitagawa, T. Nakanishi, T. Seki, K. Fushimi, H. Ito, Y. Hasegawa, *Chem. Eur. J.* **2018**, *24*, 1956–1961.

[44] K. Yanagisawa, Y. Kitagawa, T. Nakanishi, T. Akama, M. Kobayashi, T. Seki, K. Fushimi, H. Ito, T. Taketsugu, Y. Hasegawa, *Eur. J. Inorg. Chem.* **2017**, *2017*, 3843–3848.

[45] L. N. Sun, J. Yu, H. Peng, J. Z. Zhang, L. Y. Shi, O. S. Wolfbeis, *J. Phys. Chem. C* **2010**, *114*, 12642–12648.

[46] J. Yu, L. Sun, H. Peng, M. I. J. Stich, *J. Mater. Chem.* **2010**, *20*, 6975.

[47] A. Balamurugan, M. L. P. Reddy, M. Jayakannan, *J. Mater. Chem. A* **2013**, *1*, 2256–2266.

[48] D. V. Lapaev, V. G. Nikiforov, V. S. Lobkov, A. A. Knyazev, Y. G. Galyametdinov, *Opt. Mater. (Amst).* **2018**, *75*, 787–795.

[49] V. Frisch MJ, Trucks GW, Schlegel HB, Scuseria GE, Robb M, Cheeseman JR, Scalmani G, Barone V, Mennucci B, Petersson GA, Nakatsuji H, Caricato M, Li X, Hratchian HP, Izmaylov AF, Bloino J, Zheng G, Sonnenberg JL, Hada M, Ehara M, Toyota K, Fukuda R, Hasegawa, F. D. GA, Salvador P, Dannenberg JJ, Dapprich S, Daniels AD, Farkas Ö, Foresman JB, Ortiz JV, Cioslowski J, W. C. GA, Salvador P, Dannenberg JJ, Dapprich S, Daniels AD, Farkas Ö, Foresman JB, Ortiz JV, Cioslowski J, Fox DJ (2009) Gaussian 09, Revision D.01. Gaussian, Inc., *Gaussian, Inc., Wallingford, CT, USA* **2009**.

[50] R. L. Martin, *J. Chem. Phys.* **2003**, *118*, 4775–4777.

FULL PAPER

Novel seven coordinate Tb^{III} complexes with ethynyl group in phosphine oxide ligands are synthesized and their photophysical properties are investigated. The introduction of ethynyl groups promoted thermo-sensing properties through LLCT transitions while showing intense luminescence.

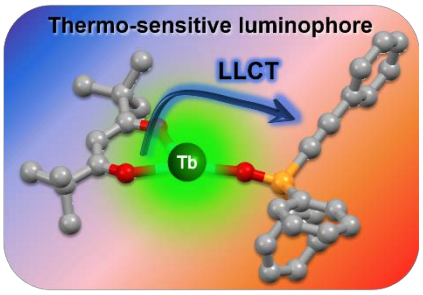

Thermo-sensitive luminophore

*Pedro Paulo Ferreira da Rosa, Takayuki Nakanishi, Yuichi Kitagawa, Tomohiro Seki, Hajime Ito, Koji Fushimi, Yasuchika Hasegawa**

Page No. – Page No.

Thermo-sensitive luminophores using seven-coordinate Tb^{III} complexes based on LLCT transition